THE ROLE OF RHEOLOGY IN EARTHQUAKE TRIGGERING AT THE MIDDLE AMERICA TRENCH IN COSTA RICA DUE TO THE MARCH 25, 1990 NICOYA GULF EARTHQUAKE

By Candy E. Elliott

Submitted in Partial Fulfillment of the Requirements for the

Master of Science in Geophysics

New Mexico Institute of Mining and Technology
Department of Earth and Environmental Science

Socorro, New Mexico

Acknowledgements

I would like to thank my committee, Dr. Susan L. Bilek, Dr. Glenn Spinelli, and Dr. Gary Axen for patiently guiding me through this process. Thanks also to Dr. Harold Tobin who helped through my first year, and to Dr. Rakhim Aitbayev for attempting to teach me the finite element method. Many thanks go to my friends at New Mexico Tech who supported me with encouragement, academic support, and childcare. You are all wonderful and amazing.

Thank you to my two children, Hunter and Elizabeth, for your love, understanding, and endurance. Thank you to my husband, Michael, for sacrificing so much so that I could pursue my dreams. Thank you to everyone at The Episcopal Church of the Epiphany for your unconditional acceptance. May God continue to bless you all. Finally, special thanks to my advisor Dr. Susan Bilek for being patient, understanding, and supportive beyond belief.

ABSTRACT: Subduction zones produce the largest earthquakes on the planet, yet the processes involved are still not fully understood. My research focuses on stress changes in subduction zone regions due to large subduction megathrust earthquakes and related triggering on adjacent faults. I investigated a large subduction zone earthquake in Costa Rica to determine if aftershocks and subsequent nearby seismicity were triggered by the earthquake. The $M_W = 7.0$ earthquake occurred in the Nicoya Gulf, Costa Rica on March 25, 1990. Using data provided by Obvservatorio Vulcanológico y Sismológico de Costa Rica (OVSICORI), which operates a local seismic network, I examined events for 90 days prior to the March 25 event as well as up to 120 days after the $M_W = 7.0$ earthquake. Using Coulomb static stress modeling software, I evaluated the Coulomb static stress changes in the region due to the earthquake and found that the majority of aftershocks lay within regions of static stress increase. I also examined an anomalous patch of delayed seismicity, which peaked in both number and magnitude of events at around 90 days after the mainshock. More than half of these earthquakes were found to lie on a single group of right-lateral strike-slip faults known as CR-25. Using 2-D finite element modeling, I examined the effects of variable rheology on the stresses in the region and found that Coulomb static stresses did increase through time inland of the trench when a viscous component was added to the lower crust. I conclude that the inland events may well have been triggered by viscoelastic relaxation of the crust due to the March 25, 1990 Nicoya Gulf earthquake.

TABLE OF CONTENTS

LIST OF FIGURES

This thesis is accepted on behalf of the
Faculty of the Institute by the following committee:

Susan L Smith

Advisor

Aug 27, 2007

Date

I release this document to the New Mexico Institute of Mining and Technology.

Carolyn E Ellis

Student's Signature

27 Nov. 2007

Date

CHAPTER 1. BACKGROUND

Introduction. The region of the Middle America trench near Nicoya Peninsula, Costa Rica has been the focus of much geophysical investigation in the past two decades. There is a large amount of seismic data from both global and regional seismic networks, as well as data from numerous scientific investigations including seismic reflection and refraction, GPS, and magnetics [*von Huene et al.*, 1995; *Hinz et al.*, 1996; *Barckhausen et al.*, 1998; *Lundgren et al.*, 1999; *Husen et al.*, 2002; *Norabuena et al.*, 2004]. These studies have identified regions of seamount subduction, specifically the Fisher seamount and Fisher ridge [*Husen et al.*, 2002].

The March 25, 1990 $M_W = 7.0$ Nicoya Gulf, Costa Rica earthquake was thought to have occurred as a subducting seamount ruptured. *Protti* [1995a] suggested that the seamounts in Costa Rica reduce the interface coupling and limit the magnitude of subduction-zone earthquakes to ≤ 7.6. A key to understanding the complexity of how topography affects the coupling strength and potential for earthquake generation is analysis of slip and resultant static stress changes associated with subduction-zone earthquakes. Since these features on the plate interface are not directly accessible, one must rely on earthquake data, seismic reflection profiles, plate motion estimates, thermal, hydrologic, and lithologic constraints to give information into the rupture process and ensuing stress changes.

In this work, I examine stress changes in the subduction zone due to the March 25, 1990 earthquake. Using two distinct modeling techniques, I have calculated Coulomb static stress change, and how static stress changes vary with fault orientation and rheology. I use these models to explore the spatial and temporal distribution of earthquake triggering in the region and to draw conclusions about the relationship of stress changes to aftershocks. The models are based on the geologic and geophysical data from the region.

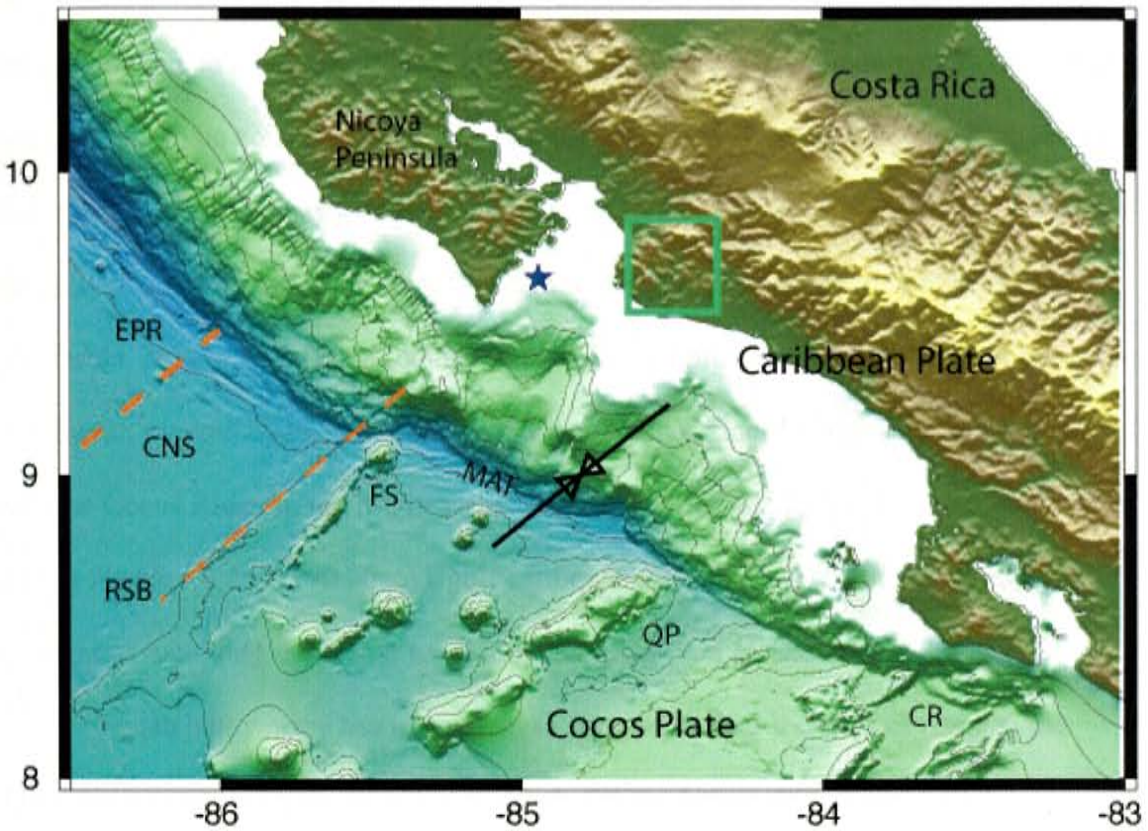

Figure 1. Costa Rica location map. The Cocos plate is being subducted beneath the Caribbean plate. Double arrow line shows the principal horizontal stress orientation from the World Stress Map. Dashed orange lines show the location of the East Pacific Rise (EPR) and Cocos Nazca Spreading Center (CNS) boundary as well as the rough-smooth boundary (RSB). Bathymetry shows the Fisher seamounts (FS), the Quepos plateau (QP), and the Cocos ridge (CR) which subduct at the Middle America Trench (MAT). The blue star shows the epicentral location of the March 25, 1990 earthquake which occurred off Nicoya Peninsula, Costa Rica. The green box indicates the area of inland triggered seismicity.

Geologic setting. Off the west coast of Costa Rica lies the Middle America trench (MAT), where the Cocos Plate is subducting beneath the Caribbean Plate (Figure 1). The rate of convergence varies from 8.4 cm/year in the northwest to greater than 9 cm/year in the southeast [*DeMets*, 2001]. At Nicoya Peninsula, the seafloor bathymetry changes from smooth in the north to rough in the south. This transition from relatively low bathymetric relief to seamount and ridge dominated seafloor relates to earthquake magnitude due to coupling strength [*Protti et al.*, 1995a]. The rough-smooth boundary was thought to be coincident with where crust generated at the East Pacific Rise (EPR) met crust formed at the Cocos-Nazca Spreading Center (CNS). The EPR/CNS boundary actually lies northwest of the smooth-rough transition, at the southern end of Nicoya Peninsula. *Husen et al.* [2003] consider three distinct provinces; a smooth segment in the northwest, marked by the smooth-rough boundary, a seamount dominated central region, and the Cocos Ridge in the southeast. The seamount dominated region, the region in which the March 25, 1990 Nicoya gulf earthquake occurred, is $\approx$ 40% covered by seamounts including the Fisher seamount and ridge [*von Huene et al.*, 1995].

Swath bathymetry has imaged these seamounts near the Gulf of Nicoya, the Fisher seamount being the most trenchward of these features[*Hinz et al.*, 1996]. The margin wedge shows significant deformation in the direction of convergence, indicating seamounts have penetrated the margin wedge and are being subducted [*Dominguez et al.*, 1998; *Fisher et al.*, 1998].

The inland area surrounding seamount subduction includes Nicoya Peninsula and regions to the southeast of Nicoya gulf. These inland regions are rife with Quaternary faults that are primarily normal and right-lateral strike-slip faults [*Marshall et al.*, 2000a]. At Nicoya Peninsula, ophiolitic rocks outcrop and contain strike-slip and normal faults. The significant uplift of the peninsula has been attributed to seamount subduction [*von Huene et al.*, 1995]. Continuing south and east, a series of fault-bounded blocks have been uplifted, the possible result of seamount subduction [*Fisher et al.*, 1998; *Marshall et al.*, 2000a].

The margin wedge consists of an ophiolitic core overlain by a thin cover of sediment, with rocks correlating in age and composition to the Nicoya Complex. There is minimal accretion here, and most of the sediments covering the oceanic plate are subducted. The dewatering of these sediments as they subduct has a significant impact on the effective stress in the system.

Earthquakes and asperities. The term asperity, initially used to describe frictional behavior by Amonton in the 17th century and later by [*Byerlee*, 1978] has been used widely with some variation in meaning, including a seismological high slip region [*Lay et al.*, 1981; *Lay et al.*, 1982; *Kanamori*, 1986a; *Cloos*, 1992; *Ruff*, 1992; *Johnson and Nadeau*, 2002, 2005]. In this text I will refer to the term "asperity" as an area of increased strength along a fault interface. The basic premise for the asperity model is that asperities form areas of strength that resist plate motion to a greater degree than the surrounding slab. When the stresses accumulate to meet failure criteria, the asperities

break and the result is an earthquake. The moment release, slip area, and stress drop are all a function of the extent and strength of the asperity.

The alternate model is known as the "barrier" model [*Aki*, 1979, 1984],which is similar to the asperity model except in the rupture process. Rather than acting as areas of rupture initiation, the barrier model suggests that zones of increased strength act as barriers to rupture propogation. The most fundamental problem with this model is its failure to accommodate plate motion. The asperity model allows for plate motion either seismically or aseismically [*Kanamori*, 1986b] resulting in earthquake rupture or aseismic slip. It is possible, and even plausible that seamounts can act as either rupture initiation zones or barriers.

Current models of subduction-zone thrust earthquakes suggest that stresses accumulate at strong patches along the fault interface and that earthquakes occur as these regions, called asperities, rupture and release energy. At the Gulf of Nicoya it was found that the subducting seamounts are acting as asperities and that the 1990 Nicoya Gulf Mw = 7.0 earthquake occurred as one of these seamounts ruptured [*Husen et al.*, 2002]. The amount of seismic moment release from these seamount zones is significantly lower than the moment released from earthquakes occurring in areas of smooth seafloor subduction [*Protti et al.*, 1995b; *Bilek et al.*, 2003].

Earthquakes and stress changes. When an earthquake such as the 1990 Nicoya event occurs, a series of aftershocks follow the larger event, referred to commonly as the mainshock. The mainshock in effect "triggers" the smaller events, and can trigger large

events either through static or dynamic stresses [*Stein*, 1999; *Steacy et al.*, 2004; *Freed*, 2005; *Parsons*, 2005; *Steacy et al.*, 2005a]. After slip on the fault relieves the accumulated stresses, the stress is lowered in that region but increased in some adjacent regions. Although the absolute stress can not be measured on a fault, stress changes can be calculated, either through Coulomb stress change criteria or rate and state friction [*Stein et al.*, 1997]. Static stress triggering can occur on an individual segment of a fault, or on an adjacent fault. Probably the most well studied example of static stress triggering on a single fault is the1997 Izmit, Turkey, earthquake [*Stein et al.*, 1997]. An example of static stress triggering on adjacent faults is the 1992 Landers-Big Bear sequence in California; the Landers earthquake caused increased stresses on the Big Bear fault, accelerating it toward failure, which occurred three hours later [*Toda et al., 2006]*.

At least a portion of the near-field events, however, are dynamically triggered. Dynamic triggering occurs as passing surface waves cause small displacements on faults which are already near failure. These earthquakes can be part of the aftershock sequence, but can also occur as events on faults which are quite far away, such as those events triggered from the Denali earthquake of 2002 [*Gomberg et al.,* 2004]. Dynamic triggering has also been suggested to be responsible for earthquakes which occur much later than those initially attributed to dynamic passage of surface waves. In this model, called "delayed dynamic triggering", surface waves cause physical disturbances to the fault interface which accelerates the recurrence interval of that individual fault [*Parsons*, 2005].

According to Omori's law, the number of triggered events in a region will decay with time after the mainshock. Occasionally, however, an anomalous group of delayed

events will occur that do not obey Omori's law. One such group occurred after the Nicoya Gulf earthquake. In an inland region approximately 120 kilometers from the trench, seismic activity ramped up in number and magnitude between 60 and 120 days after the $M_W = 7.0$ earthquake. This activity peaked at around 90 days (Figure 2). In this thesis, I explore the possibility that the stress changes that triggered these events could be related to the rheology of the region.

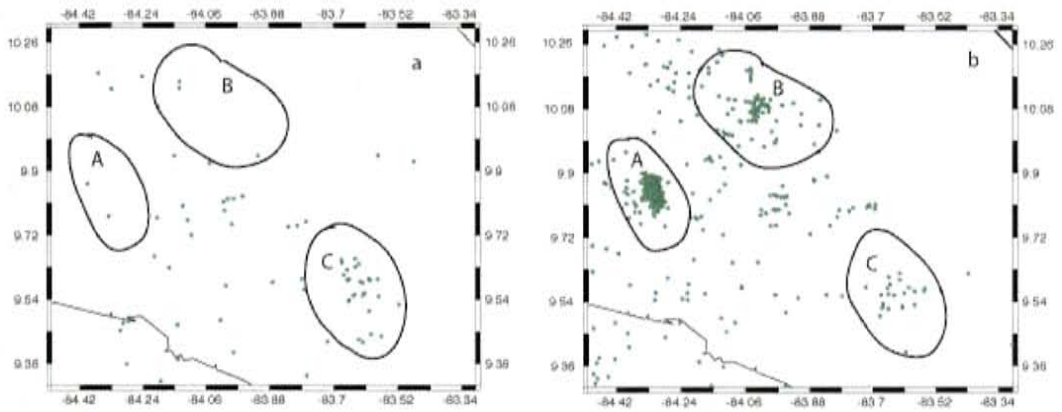

Figure 2. Inland region of seismicity. Patches of inland seismicity for 90 days before the March 25, 1990 earthquake (a) and 90 days after (b). Note that patch A shows a highly concentrated patch of increased activity, with 71 events in panel a and 397 events in panel b. This region corresponds to the box shown in Figure 1.

Rheology and stress changes. Many important stress change models have been created, particularly static stress change models. These models include the Coulomb software created by the USGS, which computes Coulomb failure stress on individual faults with specific earthquake and fault parameters [*King et al.*, 1994; *Stein*, 1999; *Lin and Stein*, 2004]. This software has been successfully used to model stress changes on faults such as the North Anatolian and the San Andreas [*Stein*, 1992; *Stein and Barka*,

1997]. Earthquake stress change models such as Coulomb use a linearly elastic homogeneous half-space to calculate stress changes. It may be argued that the crust behaves elastically to the first and even subsequent orders for earthquake repeat cycles, but linearly elastic behavior may not necessarily be an accurate assumption for all fault zones, particularly for subduction zones.

Subduction zone faults differ in stress distribution and transmission after megathrust earthquakes. Using a 3-D elastic model, [*Taylor et al.*, 1998a] found that strike-slip events may be promoted in the upper crust inland of the subduction zone event. [*Lin and Stein*, 2004], also using an elastic rheology, found that normal faulting is promoted in the outer rise of the subduction zone, up-dip of the area of slip along the interface, and that thrust events are promoted down-dip and in a small area in the back-arc, as well as along strike.

[*Honda et al.*, 2002] suggest that heat flow may be convective in back arc regions and may reduce viscosities beneath the crust by two orders of magnitude. If convection is occurring in the back arc, the down-dip region of the subduction thrust interface below the seismogenic zone could be behaving more viscously and could transfer the stresses of the aseismogenic zone into the overlying crust. Given this complexity, I take these variations into account when trying to explore the triggered Costa Rican seismicity.

It is not known how much the variation in rheologic properties with depth affects stress changes on earthquake time scales. *Ruff [2001]* suggested that for earthquake repeat time scales, one could assume a simple, two layered subduction zone interface with a linearly elastic upper layer corresponding to the seismogenic zone, and a viscous down-dip portion corresponding to the aseismic zone. The upper blocks in his model are

connected by springs, which are in turn connected to a rigid "backstop". The backstop is a mechanical boundary that is a result of composition, heat, and/or dewatering; this boundary is suggested to correspond to the trenchward limit of arc volcanism [*Byrne and Hibbard*, 1987].

As we examine the role of the variable rheology in the area, we must also look to other factors potentially affecting stresses in the subduction zone and surrounding area. The structure of the Costa Rican Pacific margin is somewhat complex. Seismic velocities in this region have been correlated to thermal convection in the back arc, further supporting lower viscosities in the down-dip aseismogenic zone. We estimate that the general area above the more viscous aseismic zone for the MAT near Nicoya Peninsula would lie approximately 130 kilometers inland from the trench axis, due to the trenchward limit of arc volcanism. The temporally anomalous events observed in the catalog lie about 120 kilometers from the trench. It is important to understand how the rheology of the region below the seismogenic zone affects stress transfer to the overlying crust.

I began the process of examining if and how stress changes were related to the rheology of the region by using an elastic half-space model, and then progressing to 2-D elastic and layered viscous and elastic finite element models. By examining the stress changes involved in the models both statically and through a series of relaxation times, I hoped to gain insight into the processes by which earthquake triggering in subduction zones occurs.

CHAPTER 2. METHODS.

Introduction. Stress change models lend insight into regions of stress increase due to seismic slip on a fault. I began my efforts with a linearly elastic half-space model, and then progressed to a two-dimensional finite element linearly elastic model, and finally a two-dimensional model with an elastic layer overlying an elastic and viscous layer. By comparing these models, I hoped to explore the controls on the stress changes in the crust as a result of the 1990 Nicoya gulf earthquake. As mentioned in Chapter 1, I wanted to understand if viscous relaxation of the upper mantle and lower crust could have been responsible for stress perturbations which in turn triggered the anomalous seismicity 90 days after the March 25 earthquake. This chapter will provide details on the stress change calculations, model development, and parameters used.

Seismological parameters. For all the subsequent model development, I need basic information about the earthquake, specifically fault orientation, location, and the amount of slip for the specific earthquake. The March 25, 1990 $M_W = 7.0$ earthquake was a megathrust event which occurred in the Gulf of Nicoya, near Nicoya Peninsula. The Global Centroid Moment Tensor (http://www.globalcmt.org/) catalog listed the strike, dip, depth and seismic moment of the earthquake as 303°, 11 °, 20 kilometers, and 1.1 * 10^{27} dyne·cm respectively. *Protti et al.* [1995a] listed the dip of the interface as 17 °. This discrepancy is likely due to the changing dip of the interface with depth as the slab bends.

The earthquake was recorded by both global and local seismic network. Local aftershock location data were provided by the Obvservatorio Vulcanológico y Sismológico de Costa Rica (OVSICORI). This catalog includes all locally recorded events over local magnitude 1.5 spanning 85 days before the March 25, 1990 event to well over one year after (Figure 3). From this data, I plotted aftershocks for 90 days following the earthquake, in order to constrain the slip area along the fault. Using the slip area of 676 km^2 from the aftershock data, I calculated the average slip of the earthquake to be 2.94 meters. This figure was calculated using the following formula:

$$M_o = GAD \qquad (1)$$

G is the shear modulus, A is the area, and D is the slip. The value of the shear modulus used was 3.0×10^{10} Pascals, a widely accepted and used value for earth materials. The required seismological parameters are provided in Table 1.

Seismological parameters		
Seismic moment	1.10E+27	dyne· cm
Shear modulus	30	GPa
Area of slip	676	km^2
Amount of slip	2.94	m

Table 1. Seismological parameters

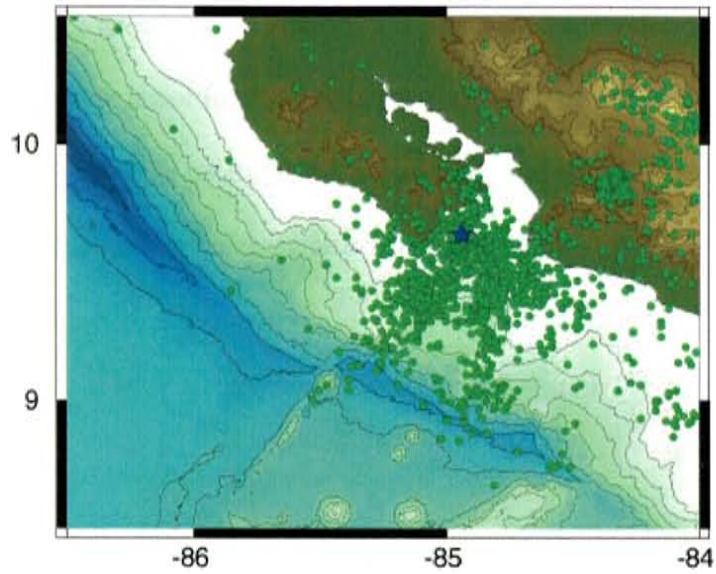

Figure 3.Nicoya Gulf earthquake and aftershock map. Epicentral location (blue star) of March 25, 1990 Nicoya Gulf earthquake and aftershocks (green dots) for 120 days after the mainshock.

Elastic half-space models. I evaluated Coulomb stress changes by using Coulomb 2.6 and the recently updated version Coulomb 3.0 software [*King et al.*, 1994; *Toda and Stein*, 2002]. These stress change calculations are based on elastic dislocation formulae to resolve stresses on receiver planes within a uniform elastic half-space. Specific fault and earthquake parameters, including strike, dip, rake, slip, slip area, shear modulus and Young's modulus are included in an input file, along with specific receiver faults. The input file is used to create a grid onto which the stress changes will be displayed after calculation (Figure 4). Orientation of the regional stress field must also be provided. This data was obtained from the World Stress Map [*Reinecker and Heidbach*, 2005]. The software is then used to calculate stress changes either on specified receiver faults listed in the input file, or on all optimally oriented strike-slip, normal, or reverse faults in the region. Optimal orientation for faults is based upon the regional stress field, the stress changes associated with the slip on the source fault, and the effective

coefficient of friction. Calculations are performed for individual points within the stress field, and rotate according to the location of the faults within the stress field. Where stress changes are low, the rotations are very small, and where stress changes are large and positive, the rotation becomes more pronounced.

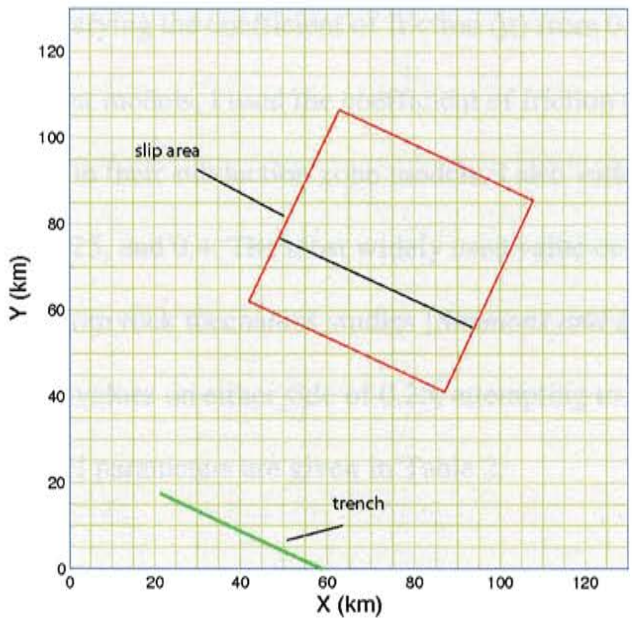

Figure 4. Elastic half-space model grid in mapview. Coulomb grid showing surface expression of the trench and area of coseismic slip. The black line in the slip area indicates the position of intersection of the fault at this calculation depth (20 km).

To quantify the stress changes that occurred in response to the March 1990 event, we used Coulomb failure criteria, in which Coulomb stress ($\Delta\sigma_f$) is related to the friction coefficient (μ), the change in effective stress (the changes in pore pressure (Δp) and normal stress ($\Delta\sigma_n$)) and the changes in the shear stress ($\Delta\tau$). This relationship is defined by the formula:

$$\Delta\sigma_f = \Delta\tau + \mu(\Delta\sigma_n + \Delta p) \qquad (2)$$

I explored the effects of a range of variables on the Coulomb static stress changes. The software Coulomb 2.6 allows us to test a variety of frictional parameters, and provides several options for resolving stress change onto different receiver faults. I examined the effect of varying the coefficient of friction (μ) from 0.0 to 1.0 in 0.2 increments. In subsequent models, I used the coefficient of friction 0.4 which was used by *Lin and Stein* [2004] in their subduction zone models. I also varied Poisson's ratio, using the values 0.15, 0.25, and 0.4. The most widely used value of Poisson's ratio is 0.25, a value obtained from rock mechanics studies [*Simmons and Brace, 1965*]. For completeness, we chose values on either side of 0.25, attempting to stay within reasonable values. Model parameters are given in Table 2.

Coulomb 2.6 model parameters

Principal stress orientation	**Constants**
$\sigma 1 = 27.00°$	Poisson's Ratio = 0.25
$\sigma 2 = 113.98°$	Coefficient of friction = 0.40
$\sigma 3 = 30.02$	Young's modulus = $8.00 * 10^5$ bars
Fault parameters	**General parameters**
Dip = 17°	Calculation depth = 20 km
Slip = 2.34 meters (reverse)	Exaggeration for displacement and distance = 1000
Fault type = Optimum strike-slip	

Table 2. Elastic half-space model parameters.

2-D Finite Element Models. To test the possible effect of viscoelastic relaxation on the stress changes due to the 1990 Nicoya earthquake, we utilized ABAQUS, a commercially available finite element modeling (FEM) software. ABAQUS is a very flexible tool, which is being increasingly utilized in the geosciences; so much so that professional meetings are offering specific sessions dedicated to geologic and geophysical uses of the software. Other authors have effectively used ABAQUS to model faults with multiple layered rheology [*Kenner and Segall*, 1999; *Masterlark et al.*, 2001; *Masterlark*, 2003]. For our region, we created a 2-D model which approximates the fault geometry, with both elastic and layered elastic and viscous parameters.

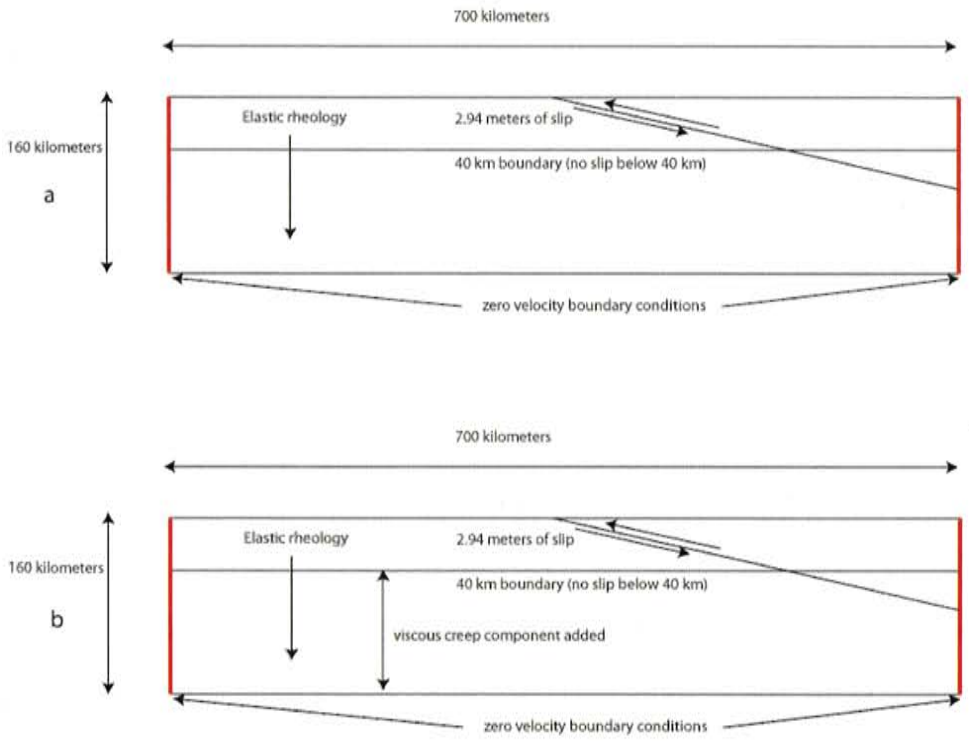

Figure 5. FEM 2-D model grid. Depiction of the elastic (a) and layered elastic and viscous (b) models.

Each of the two models was assigned elastic material properties throughout the entire model. The elastic model was assigned no further rheologic properties. The layered model was divided into an upper 40 km linear elastic layer and to the bottom 120 km layer a viscous creep component was added (Figure 5). Parameters are shown in Table 3. I chose 40 kilometers to approximate the down-dip limit of the seismogenic zone [*DeShon et al.*, 2006]. To simulate the fault interface, we chose the tangential sliding option in ABAQUS CAE, with a friction coefficient of 0.4. The value for dynamic viscosity used was 5.6 x 10^{19} Pa·s. I used power-law creep with values of n=1 and m=0, for the orders for strain and time respectively[*Kenner*, 2000], shown in equation (3). These equations are found in the "creep" material options in ABAQUS, and by using n=1, we effectively make the relationship linear, similar to Maxwell's linear viscosity.

$$\bar{\dot{\varepsilon}} = \left(A\tilde{q}^{n}\left[(m+1)\bar{\varepsilon}^{cr}\right]^{m}\right)^{1/(m+1)} \qquad (3)$$

$\bar{\dot{\varepsilon}}$ is the uniaxial equivalent strain rate, $\bar{\varepsilon}^{cr}$ is the uniaxial equivalent creep rate, $\tilde{q}$ is the uniaxial equivalent deviatoric stress, and A, m, and n are user defined quantities dependent on viscosity, time, and strain, respectively.

I experimented with a range of displacement conditions. Initially I used simple velocity boundary conditions and then progressed to a slip on the fault interface equivalent to the slip that occurred during the Nicoya Gulf earthquake. The blocks were initially displaced by a velocity boundary condition in the x-direction corresponding with a convergence rate of 8.5 cm/yr. This velocity was divided equally between the two blocks. Next, I resolved the amount of coseismic slip from the 1990 Nicoya earthquake onto the contact surface of the model. I then tested the models with the velocity boundary

conditions alone, the velocity boundary conditions with the slip, and the slip alone. The velocity boundary condition model tended to concentrate the stress changes at the edges of the model. The model with both velocity and slip resolved the stresses onto the faults more appropriately, and the model with slip alone resolved the stress changes on the fault with negligible change compared to the model with both velocity and slip boundary conditions.

Model 1:Elastic		
Elastic parameters		
Material	**E in Pa(N/m^2)**	**ν**
Continental crust	5.60E+10	2.50E-01
Oceanic crust	8.00E+10	2.50E-01
Mantle	1.50E+11	2.50E-01
Boundary conditions		
Displacement in meters	2.94E+00	
*Velocity in cm per year	8.50E+00	
Model 2: Elastic and viscous		
Elastic parameters		
Material	**E in Pa(N/m^2)**	**ν**
Continental crust	5.60E+10	2.50E-01
Oceanic crust	8.00E+10	2.50E-01
Mantle	1.50E+11	2.50E-01
Viscosity (below 40 km only)	5.16E+19 Pa-sec	
Boundary conditions		
Displacement in meters	2.94E+00	
*Velocity in cm per year	8.50E+00	

Table 3. FEM parameters. *Note that the velocity boundary condition was not used in the final model.

The layered FEM (panel b in Figure 5) was run for five increasing time steps to allow examination of the stress changes at each of the elapsed time periods. I began at t = 1 second and increased the time to nine days, ninety days, 900 days, and 9000 days respectively. I allowed the model to run well into the future to explore possible thresholds for triggering, as well as reasonable earth value restrictions.

CHAPTER 3. RESULTS.

Introduction. The results from this project can be separated into three general categories; the elastic half-space model, the elastic FEM, and the layered viscous-elastic FEM. The differences in methodology make direct comparison of the elastic half-space and FEM difficult. I have attempted to highlight the similarity of the model parameters and geometry; however, it is essential to note that, unlike the half-space model, the FEM is calculated in two dimensions only, and lacks the input of site-specific parameters such as the regional stress field, and gravity load. Within this context, I explain the results of the models individually, and in a later section compare them.

Elastic half-space model. The depth of calculation for this model corresponds to the hypocentral depth (Global CMT catalog) of 20 kilometers. Maximum Coulomb static stress increase is approximately 2.4 bars. The stress changes are resolved onto optimally oriented strike-slip fault planes [*Steacy et al.*, 2005b]. Stress change results are shown in mapview (Figure 6), at individual depth slices (Figure 7), and in cross-section (Figure 8) Using these three figures we can assess the stress change lobes in three dimensions around the fault. An examination of earthquakes within discrete depth bins finds the majority of events after the mainshock fall within the lobes of static stress increase (Figure 7). Within the first 24 hours after the mainshock, we have 83% of events (88 out of 106 total) within regions of stress increase, increasing to 86% within 48 hours (171 out

of 198). The results for the range of Poisson's ratio and coefficient of friction are shown in Figures 10 and 11.

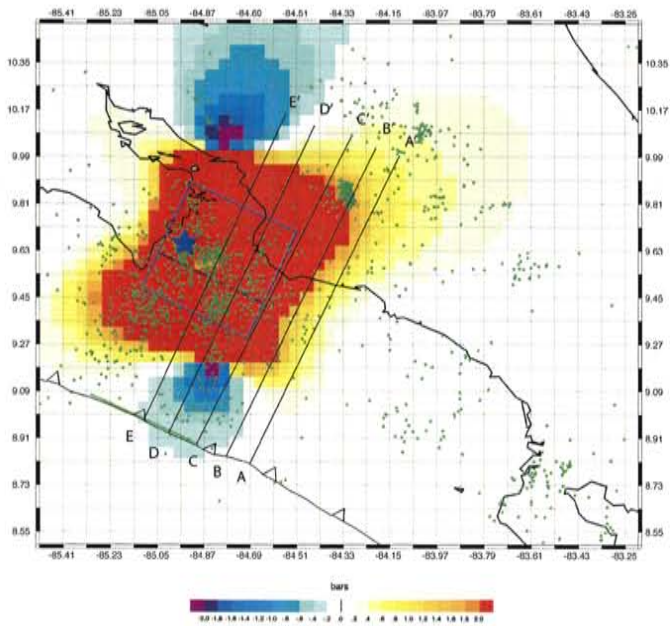

Figure 6. Stress changes in mapview. Coulomb static stress changes for optimally oriented strike slip faults overlain on Nicoya Gulf region. Blue star is the epicentral location of the March 25, 1990 earthquake; green dots are aftershock activity for 120 days after the mainshock. Blue square shows area of slip. Calculation depth is 20 kilometers.

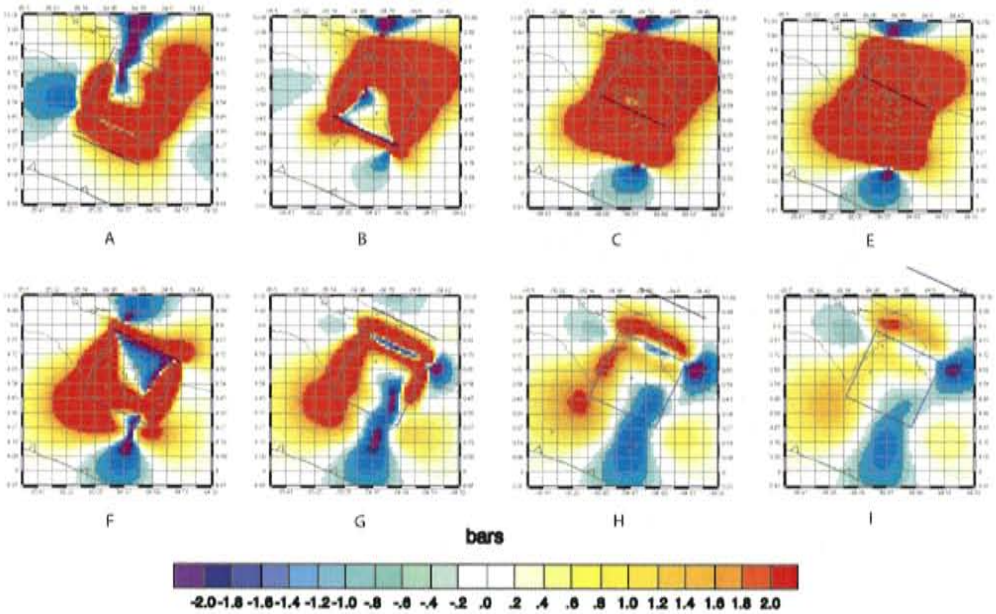

Figure 7. Stress changes in depth slices. Coulomb static stress changes for depth slices with corresponding aftershocks overlain.

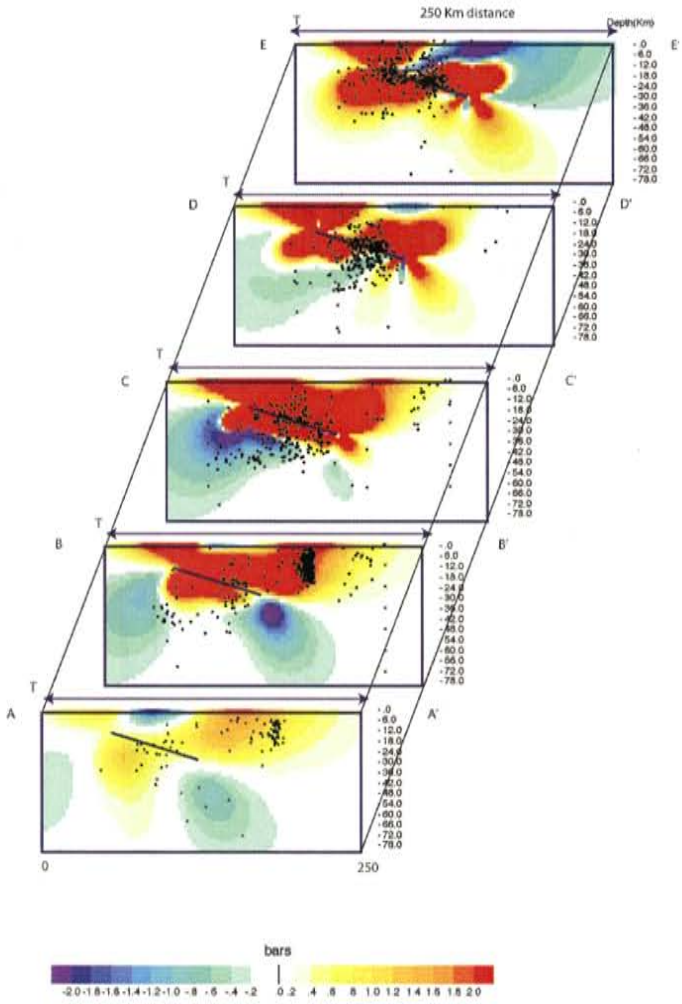

Figure 8. Stress changes in cross-section. Coulomb static stress changes in cross-section. Lines A-E correspond to the lines shown in Figure 3. Line B shows area of concentrated triggered seismicity.

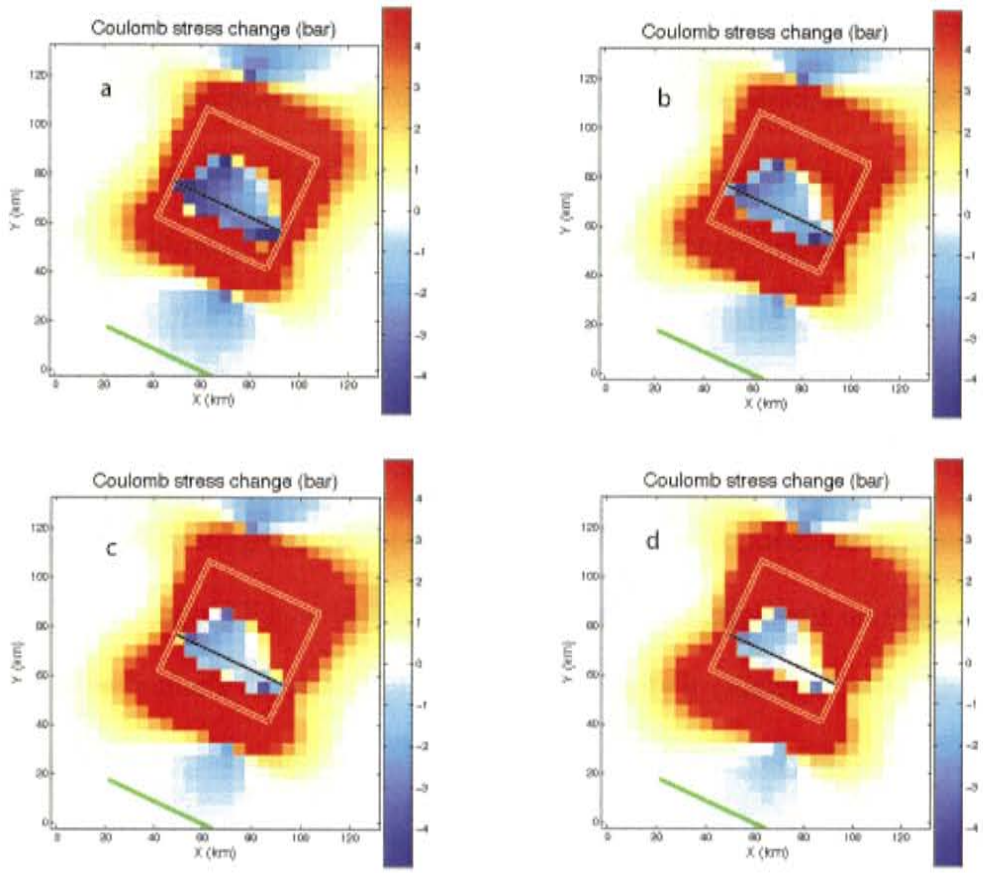

Figure 9. Variable friction models. Coulomb models with variable coefficient of friction at 0.20 (a), 0.40 (b), 0.6 (c), and 0.8 (d).

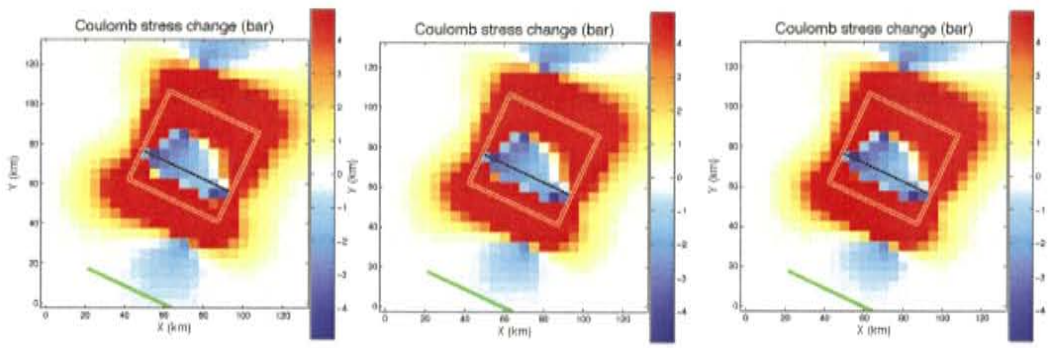

Figure 10. Variable Poisson's ratio models. Coulomb models with variable Poisson's ratio. Poisson's ratios are 0.15 (a), 0.25 (b), to 0.40 (c).

The initial models used the optimum thrust and optimum fault options in Coulomb for the resolution of stress changes as these are reasonable planes for the earthquakes on the megathrust. However, geologic surveys of the region suggest that the primary faulting in the inland region for which we propose triggering is actually strike-slip [*Marshall et al.*, 2000b]. When I revised the model using the strike-slip option [Stein, 2005, personal communication] I found that the Coulomb stress changes were more positive in the areas of aftershocks and triggered events away from the source fault, strongly suggesting that this option most closely corresponds to the seismicity patterns in the inland region (Figure 6). Optimally oriented strike-slip faults are shown in Figure 11.

A particularly dense area of increased seismicity is coincident with CR-25, a mapped quaternary right-lateral strike-slip fault, which is oriented very closely to the optimally oriented right- lateral strike-slip faults for the region (Figure 12) [*Marshall et al.*, 2000a]. The activity on this fault increased within hours after the March 25 earthquake, but did not peak in activity and cumulative seismic moment (M_o) until around 90 days after the main subduction zone event. The Coulomb static stress on the fault was increased by the earlier large event by approximately 2 bars, yet the Coulomb static stress increases does not account for the delayed increase in activity (Figure 8).

Seeking an explanation for the time delay in the region of inland triggered events, I looked to previous studies of triggered seismicity in and around subduction zones. It has been shown that time dependent subduction zone earthquake triggering can be found in the outer rise [*Taylor et al.*, 1996], as well as in strain partitioned strike-slip forearc faults [*Taylor et al.*, 1998b]. Our study correlates upper crust inland seismicity in an area that is not considered to be strain partitioned, thus we eliminated these possibilities. Some

studies have suggested that variable rheology may affect the earthquake cycle and contribute to delayed triggering.

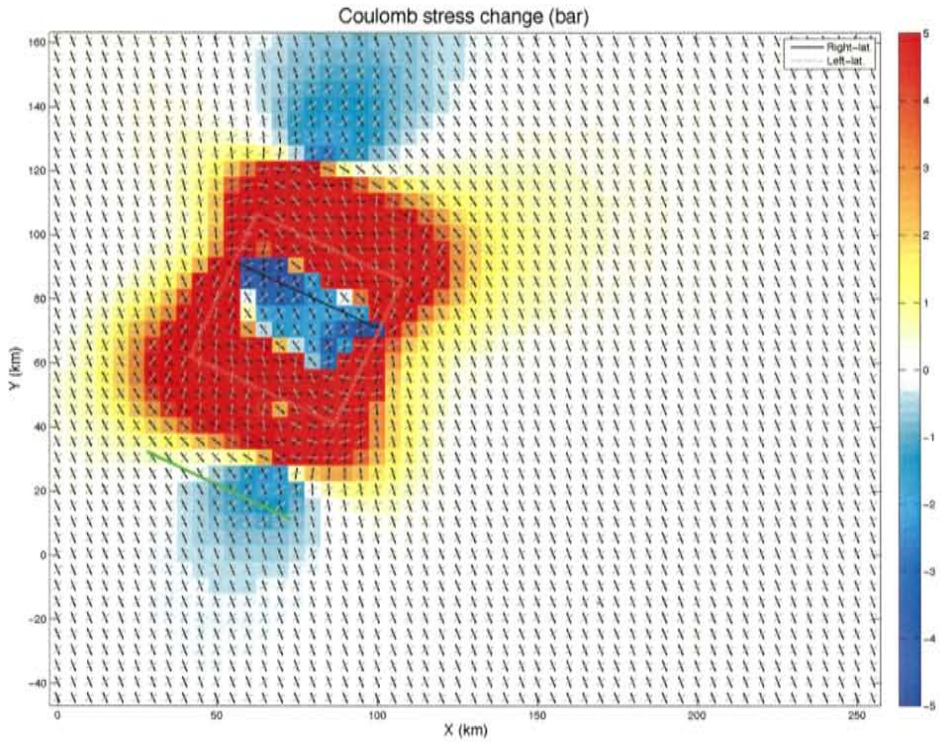

Figure 11. Optimally oriented strike-slip faults. Coulomb static stress changes for optimally oriented strike-slip faults with the orientation of these faults overlain.

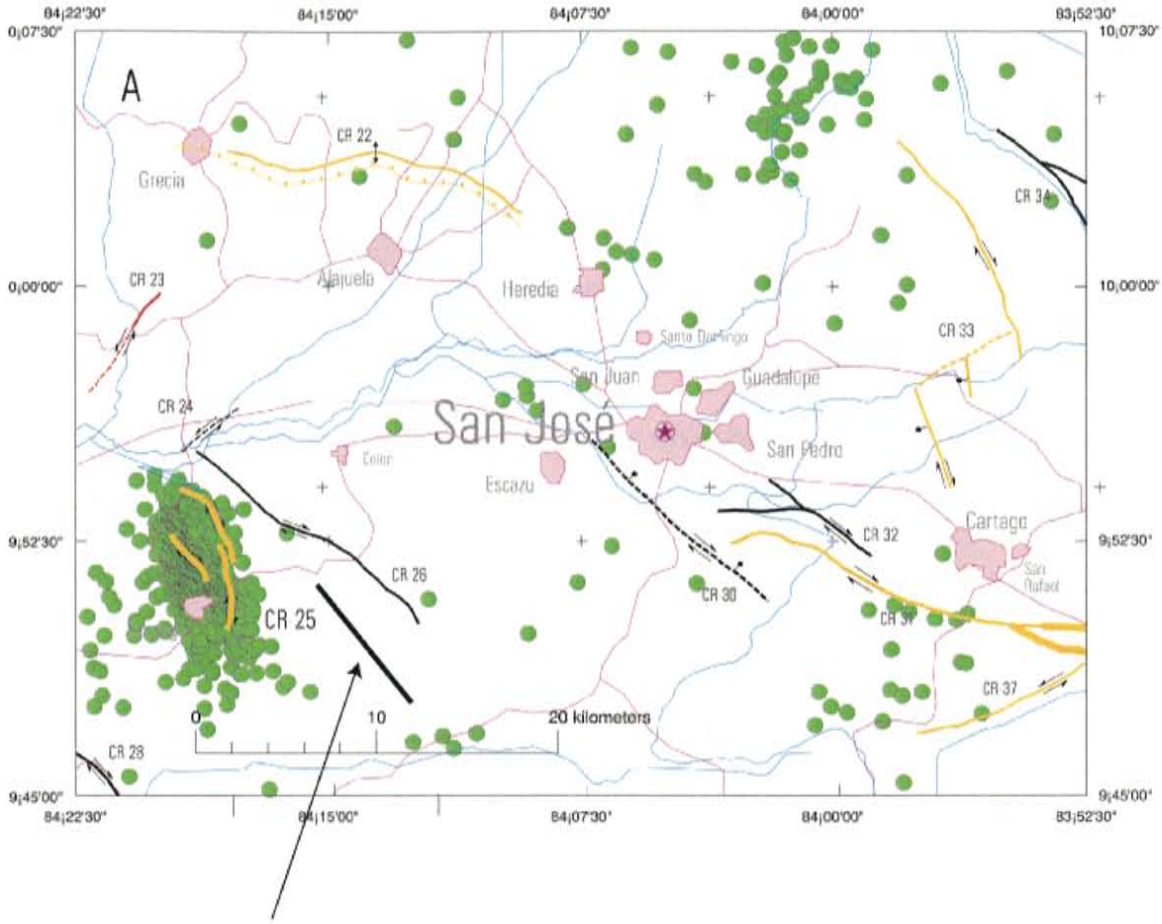

Figure 12. Fault map of inland seismicity region. This area corresponds to the boxed area denoted in Figure 1. Note the high concentration of seismicity on fault CR-25, and the orientation of the fault relative to the optimally oriented fault.

It has been suggested that patches of inland seismicity were triggered by the March 25, 1990 event [*Protti et al.*, 1995c]. There is an increase in seismic activity in two of these areas, marked *A* and *B* in Figure 2, the third, marked C, is less conclusive. Each denoted area falls within a region of Coulomb static stress increase; with A showing the

most marked increase in activity and stress increase of 1 to 2 bars as shown in the cross section line B through the seismic activity and stress change model (Figures 2 and 9).

Finite Element Model. The ABAQUS FEM, unlike the Coulomb half space model, does not return values in terms of Coulomb stress change. Graphically, ABAQUS displays von Mises stresses by default, while individual stress change values, such as σ_{11}, σ_{22}, and σ_{12}, are given in a results file. von Mises stress can be described as the measure of the magnitude of the deviatoric stresses. To compute the Coulomb stress changes in the FEM, I created a script in Matlab (Appendix B) and used the output values from the FEM and formula (2). To assign a location for each reported stress change result from the FEM, I computed the average nodal location for each element and found the corresponding Cartesian coordinates of the nodes. Normal and shear stresses were calculated using the following formulae.

$$\sigma_n = (\sigma_{11} + \sigma_{22}) - (\sigma_{11} - \sigma_{22})/\cos(2\Theta)/2 + \sigma_{12}(\sin 2\Theta) \qquad (3)$$

$$\tau = (\sigma_{11} - \sigma_{22})/\cos(2\Theta) + \sigma_{12}(\sin 2\Theta) \qquad (4)$$

σ_n is the normal stress, which is the stress normal to the contact surface, σ_{ij} are the two-dimensional stress components obtained from the FEM results file, and Θ is the angle of the fault. When calculating Coulomb stress change on strike-slip faults within the region, I used an angle of 91°.

I initially computed the von Mises stress changes in the linearly elastic FEM; as shown in Figure 13. Coulomb static stress changes are shown in Figure 15, and the elastic

FEM is compared to the elastic half-space model in Figure 15. Computed values of Coulomb stress change in the FEM are somewhat different than in the half-space model, as are the lobes of stress increase and decrease. It is clear, however, that stress increases along the fault plane increase in both models, and the general comparison of the two models lends increased significance to the work, despite the differences mentioned in the introduction to this chapter.

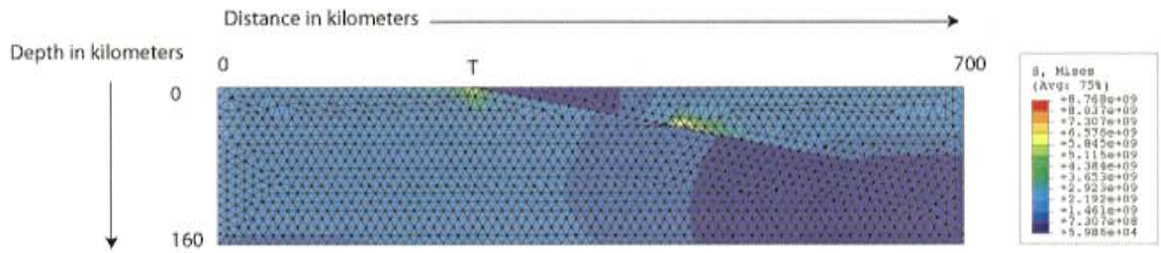

Figure13. Linearly elastic FEM. Linearly elastic FEM von Mises stress changes. T marks the location of the trench.

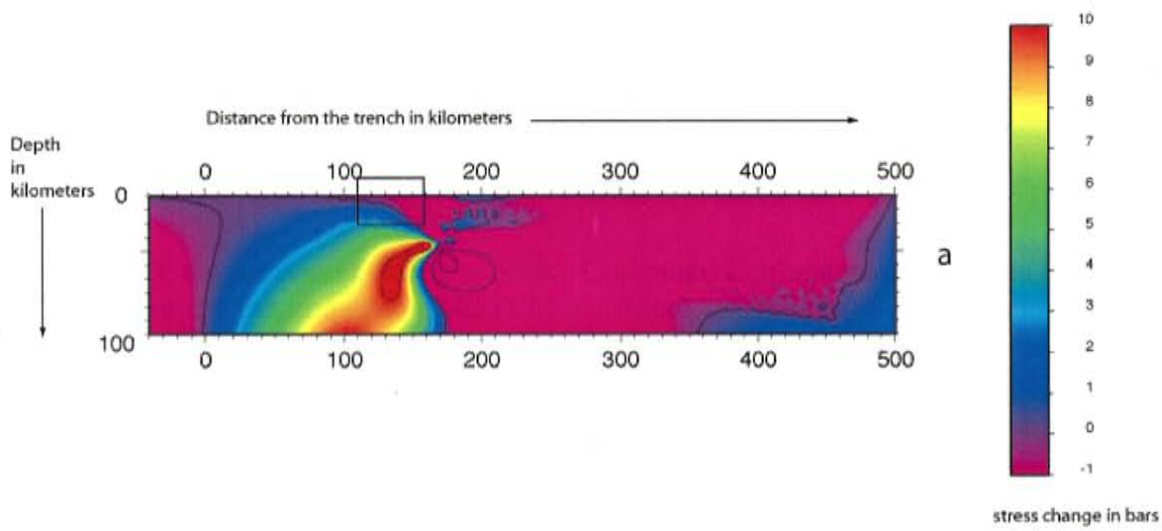

Figure 14. Elastic FEM Coulomb stress changes. Calculated Coulomb stress change from linearly elastic FEM at one second(a), nine days(b), and 90 days (c).

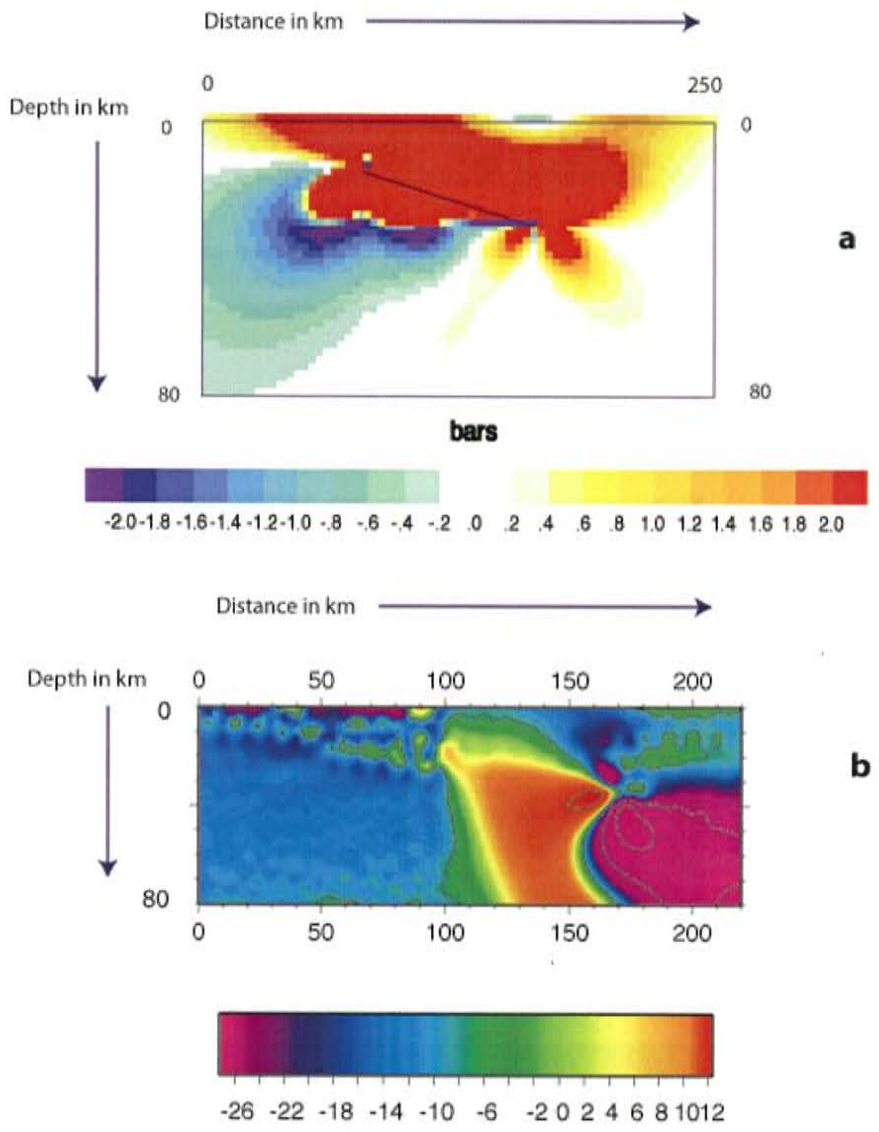

Figure 15. Comparison of elastic models. Computed Coulomb stress changes in elastic half-space model (a), and elastic 2-D FEM (b). Panel a is from cross-section line C in figure 7.

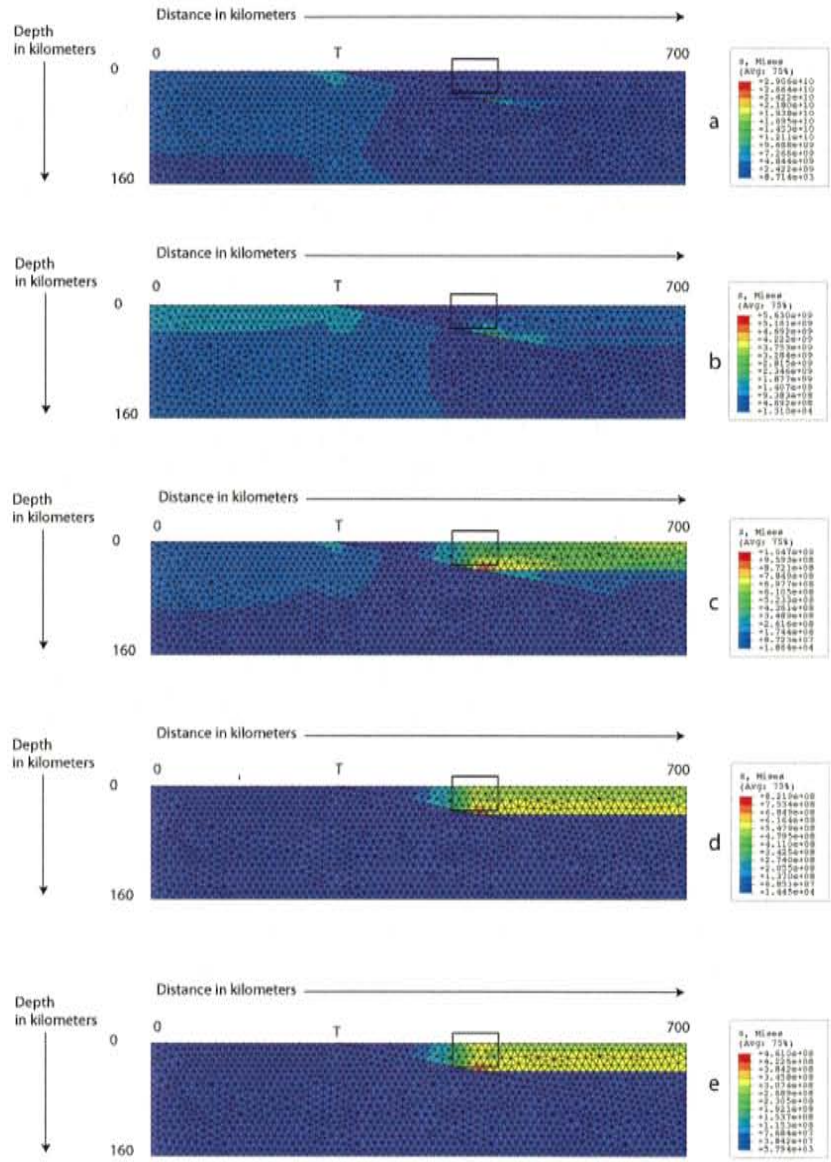

Figure16. Layered viscous/ elastic FEM. Layered viscous/elastic model von Mises stress changes through time. T marks the location of the trench in the model, and the box shows the location of the inland triggered seismicity. Timed runs are (a)one second(b)$7.776*10^4$ seconds (9 days), (c) $7.776*10^5$ seconds (90 days), (d) $7.776*10^7$ seconds (900 days) and (e) $7.776*10^8$ seconds (9000 days).

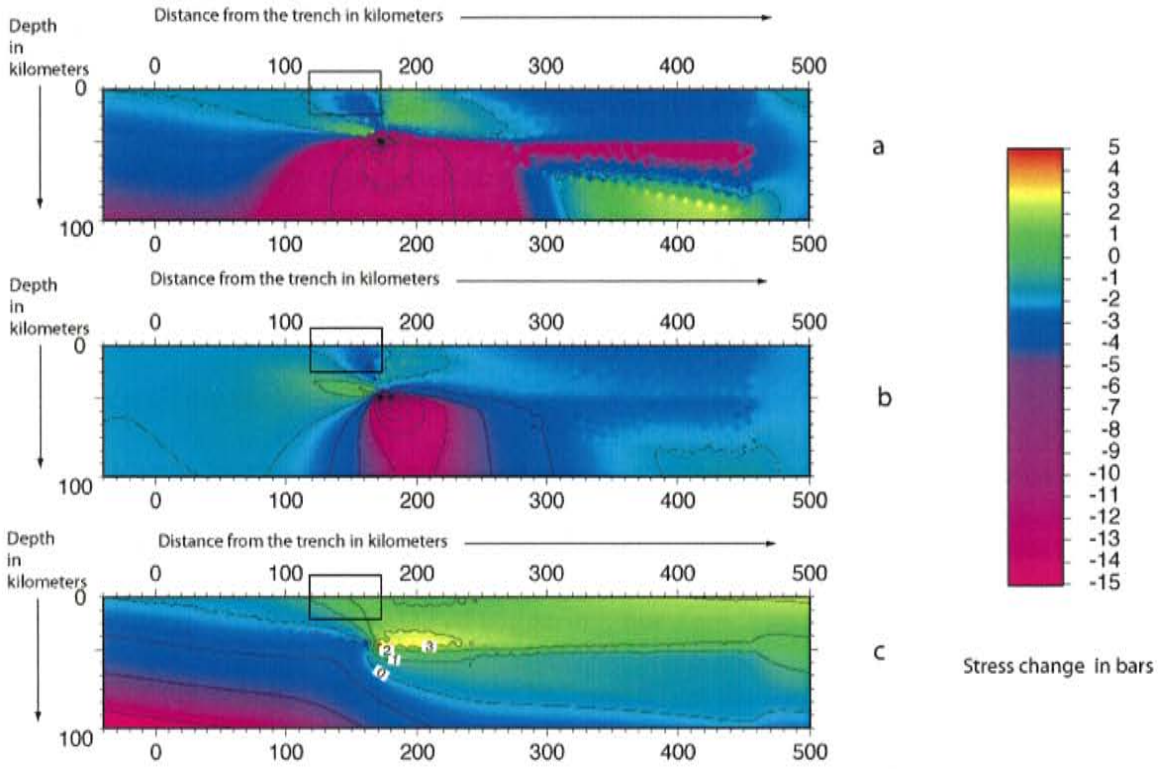

Figure17. Layered viscous/elastic FEM Coulomb stress changes. Calculated Coulomb stress changes for layered viscous-elastic model at time steps of <one day (a), 9 days (b), and 90days (c). Boxed area denotes area of increased inland seismicity. Stresses in this region increase from around -1 bar to +1 bar during the 90 day period of relaxation.

In the layered model, both the von Mises and Coulomb static stress changes increased with time, particularly in the area approximately coincident with the area of delayed seismicity increase (Figures 15 and 16). I experimented with a range of viscosities, an order of magnitude higher and an order of magnitude lower than the chosen value of $5.6 * 10^{19}$ Pa-sec. The stress transfer distribution through the time steps was identical to that of the preferred viscosity model. In the region of inland triggered seismicity, the stresses increased much more with the lower viscosity and less with the higher viscosity. The range of values for the chosen viscosity of $5.6 * 10^{19}$ Pa-sec tends to yield stress change

values of an order more comparable to the elastic half-space model stress changes. As shown in Figure 15, in the model with a lower viscous creep component the von Mises stresses are very rapidly transferred to the upper 40 kilometer elastic layer. In Figure 16, there is a contour line outside the boxed area in the increasing x-direction. This contour line shows a decrease in static stress. This may be a model artifact, or could be due to the lack of a realistic backstop in the model.

What is key here is the increase in stresses in the layered model. We know that Coulomb static stress increases are modeled for the area in question, but this does not necessarily explain the time delay of triggering, nor does it accurately reflect the actual rheology of the setting. Although it may be argued that the earth behaves elastically on earthquake time scales, to ignore the effects of increased heat in the back arc, as well as friction and mineral phase change thermal energy production, is to negate the effects of these processes on the transfer of stresses.

CHAPTER 4. DISCUSSION.

The lobes of Coulomb static stress increase correlate to both aftershocks and inland triggered seismicity (Figure 3). We show here, in accordance with other studies of Coulomb static stress change, that the stress changes induced by large subduction zone earthquakes, specifically here for the March 25, 1990, M_W = 7.0 earthquake, increased seismicity in areas of increased Coulomb static stress. This corresponds to a majority of the aftershocks (83% and 86% for 24 and 48 hour periods, respectively) being located in the zone of 0.4 to 2.0 bars of Coulomb static stress increase.

Static stress increases also extend to include areas of inland-triggered seismicity. The question is, then, why does increased inland seismicity peak at 70-90 days after the main event? Increased static stress alone does not explain the time-dependence. Using the FEM, however, we were able to show the temporal stress changes which could affect the delayed seismicity in the region. Coulomb stresses increased from -0.5 bars for the inland region at less than one day to >2.0 bars for the same region at 90 days relaxation time in the viscoelastic model which was run for the equivalent of 90 days (7.776×10^6 seconds) after the initial displacement. If the rheology behaves purely elastically and stresses decrease with time, it would be expected that the triggered seismicity in the region would follow Omori's law, and decrease linearly through time. In this study, it does not. Some researchers have suggested that thresholds for static stress failure may be 0.1 bar or lower

[*Ziv and Rubin*, 2000], so these calculated values found here are consistent with triggered events.

There is some difficulty in direct comparison of the Coulomb 2.6 model with the FEM. Tectonic stresses, gravity, and regional stress fields are lacking and are represented in the FEM as simple velocity boundary conditions. To simulate the interaction between the plates, we divide the convergence rate between equally between the overriding and underthrusting plates and use a displacement of 2.94 meters along the fault interface. One problem that presents itself is how far from the interface to end the model blocks and assign the velocity boundary conditions. Sensitivity analysis shows that this distance does influence the results of the FEM, particularly when slip along the fault is not included. Making the distance half as long results in stress increases two orders of magnitude greater than those shown in the currently described models. The backstop is a mechanical boundary that is a result of composition, heat and/or dewatering, and has been suggested to correspond to the trenchward limit of arc volcanism [*Byrne and Hibbard*, 1987]. In this region of Costa Rica, we estimate the limit of arc volcanism to be approximately 180 kilometers from the trench. I chose to extend the blocks well beyond the backstop to avoid the accumulation of stress at the ends of the model, which obscures the stress changes in the region above the faults corresponding to regions of stress change due to slip on the interface.

The Coulomb static stress change results for the elastic FEM were, as mentioned, an order of magnitude higher than the half-space model. A number of factors could be influencing these results. Most obviously, perhaps, is the limitation of the FEM to two dimensions. Calculations in a plane are often a good qualitative assessment of stress

distribution, however they lack the quantitative accuracy of a three dimensional model. One of the factors that has not been incorporated into the current 2-D model is gravity. It would be erroneous to assume that the normal stresses on the fault plane would not be influenced greatly by gravity forces. The effect of the backstop on stress accumulation may also be a factor which influences the three dimensional system.

Of the two ABAQUS models, the more realistic is the two-layered elastic/viscous creep model. Although we know that seismic waves propagate through what can be approximated as linearly elastic earth materials, we also realize that in subduction zones, pressure, temperature, composition, and pore fluid pressure can change dramatically with depth. Simplifications must always be made in modeling, and by reducing the subduction zone to two simple rheologies, we do not reflect the extreme complexity of the system. We do, however, attempt to explain the relationship of visco-elastic relaxation to stress changes within the region. And although linearly elastic models do a good job of modeling static stress changes, they fall short when attempting to constrain events such as the delayed triggered seismicity seen after the March 25, 1990 Nicoya Gulf earthquake.

The results show that in the viscous creep layered model, there is a definite increase in Coulomb failure stress through time, which is indeed what we believe to be happening. From the time of slip to 90 days after the earthquake, the Coulomb static stress changes in the layered model are 2.5 bars, well beyond the threshold for static stress triggering. These stress increases could well have caused the delayed triggered events which occurred on fault CR-25.

To better constrain the magnitude of the viscous layered model stress increases with time, we need to determine where the stress increases are most concentrated and how long it takes for the stress levels to reach critical values that lead to earthquakes. Did viscous relaxation enhance the failure of the CR-25 after the 1990 Nicoya Gulf earthquake, or did some other mechanism, such as delayed dynamic triggering, accelerate the fault toward failure? Most likely, a number of factors influenced the stress field and the failure criteria for fault CR-25, but this study suggests that a viscous lower crust and mantle could cause Coulomb failure stresses to increase with time, well within the time scale for triggering in the CR-25 events.

Suggestions for future work. The next step was to create a 3-D model that could more closely approximate the actual subduction zone, and introduce the seamount as a region of increased friction. This step was accomplished by creating a three dimensional model in ABAQUS that approximates the subduction zone and interface geometry. I began by looking at the 1990 earthquake parameters, as well as the geometry and rheology of the MAT in this region. Naturally, many simplifications were needed. The dip angle of the subduction zone thrust is approximately 11° near the trench. As the distance from the trench increases (landward), the angle of the interface increases. To model this, I used a curved interface between an "upper" and "lower" block, which initiates at an angle of 11°, and increases down dip. The upper layer of both blocks was assigned a linear elastic rheology. This region extends to 40 kilometers depth, or the approximate down-dip limit of the seismogenic zone [*DeShon et al.*, 2006]. Below this region, we used a linear viscoelastic rheology, with an effective viscosity of 5e19 Pa s.

Although this value is low for the mantle, the subduction zone seismic interface can reasonably assumed to be lower than the surrounding mantle.

Our seamount was simulated by an increased patch of friction on the lower plate interface at 20 kilometers depth. This circular patch is scaled to be the equivalent of a 2 kilometer diameter feature, roughly corresponding with the diameter of known seamounts in the region. The resultant stress changes in the model after timed runs show stress increases landward of the simulated asperity. The normal and shear stresses increase proportionally with time and subsequently so does the Coulomb failure stress. ABAQUS does not report stress changes in terms of Coulomb stress changes, and so we have calculated these from the model output normal and shear stresses.

Meshing proved to be a significant obstacle to the stability of the 3-D model. Using the "built-in" meshing options in ABAQUS CAE resulted in meshes that were either distorted or incompatible. Using these options I was unable to create a stable model; the solutions contained one or more negative eigenvalues. The graphic results show significant lack of symmetry, and should not be considered valid. Many ABAQUS users employ meshing programs, which eliminate the distortion of the mesh and allow for more valid results. Meshing programs are available commercially, although they are expensive. Academic users are creating their own meshing programs, with a great deal of success. Continued support of ABAQUS use in the Geosciences, including workshops and special sessions dedicated to use of the program, are helping to solve difficulties such as meshing issues.

CHAPTER 5. CONCLUSIONS.

Coulomb static stress models clearly show the region of inland triggered seismicity to have been in a region of static stress increase due to the March 25. 1990 Mw= 7.0 Nicoya Gulf earthquake. My findings indicate that stresses in the crust do increase with time at areas some distance away from a large earthquake as the crust is allowed to relax viscoelastically. This is a possible explanation for the delay in triggering which occurred after the March 25, 1990 earthquake in the Nicoya Gulf, Costa Rica.

This study shows that although static stress change models such as Coulomb 2.6 do a good job of showing regions of static stress increase on adjacent faults and fault segments after a large earthquake, more complex rheological models are needed to examine temporal relationships between stress transfers. Using ABAQUS finite element modeling, we found that in a simple, two-dimensional model with two distinct rheologies, stresses appear to increase in the crust with time as a function of viscous relaxation. The changes over time (90 days in our model) were $\approx$ 2 bars; we know that even much smaller perturbations may trigger earthquakes. I suggest that the increased patch of seismicity may have been caused by stress increases such as these, but more research is necessary to better constrain this relationship.

APPENDIX A

Creating the ABAQUS model (2-D)

The first step in finite element modeling is to create the geometry. The ABAQUS tutorial gives step-by-step instructions for creating given structural geometries, but approximating geologic constructions requires some trial and error. I began the process by using simple two-dimensional block geometry. My first attempts used a rectangle 250 km by 80 km, partitioned with a narrow strip which was drawn at an angle of 17 degrees from the horizontal, coincident with the angle of subduction near Nicoya Peninsula. A simple velocity boundary condition was used, and the model was run. The upper block was deformed disproportionately, and the model was revised. I initially tried using the ABAQUS gravity load feature, but without an opposing force, the block collapsed. I then tried applying a body load, which helped but did not entirely solve the problem. The solution I settled on was extending the block size to 700 km by 160 km, which eliminated the "edge effects" on the model. I later discovered that this model did not yield the results that I wanted, as all the stress was accumulated in the strip separating the two blocks.

My next attempt was to use the same basic geometry, but to create two separate portions of the rectangle and assemble them. The contact surfaces were assigned frictional parameters, which included finite sliding, and a friction coefficient of 0.4. This

geometry worked well, allowing me to compare elastic and viscoelastic response in the blocks. The following are steps used to create the working geometry.

1. Create new model.
2. In the model tree, double click part
3. Rename the part "lower block" (It makes the process easier if they are named rather than using the default "part 1", "part 2", when other properties are assigned.)
4. In the Create part dialog box, chose 2-D, shell, approximate size 800. Each of the blocks are shown below with the dimensions.
5. Using the line segment draw tool, create a vertical line at the left of the grid 160 units long; create a second line at a right angle to the bottom of the first segment 700 units long. Center click.
6. Choose the angle tool, set angle at 163 (180 – 17 = 163) degrees. Place angled line as shown in image. Center click.
7. Chose line segment tool. Connect the rest of the lines to produce the image shown. Click finish.
8. Double click part again; use the same method as described for the lower block, naming this part "upper block".

Materials

- Material 1- 5.6e10 Pa and 0.25 (upper block)
- Material 2- 8.0e10 Pa and 0.25 (lower block)

Sections

- Section 1 – material 1, plane strain thickness = 1
- Section 2 – material 2, plane strain thickness = 1

Assembly

- Instances
- Instance each part
- Position Constraints
- Edge to Edge (choose upper edge of each part)
- Edge to Edge (choose right side edge of each part)

Steps

- Create a step by double clicking- name or leave as Step 1
- Chose "visco" step
- Specify time (remember to convert to units being used in other calculations)
- Specify strain error tolerance

Interaction/ Interaction property

- Choose surface-to surface contact, chose master and slave surfaces, select finite sliding
- Choose tangential behavior, with a friction coefficient of 0.4, leaving the rest of the values as default

Meshing

- Select seed (you may need to refine the default number of seeds) and seed each part
- Select mesh type (for this geometry tet works well) and mesh each part

Boundary Conditions

- Choose lower block in edit region
- Uniform distribution
- Chose the type of boundary condition from the dialog box
- Check V1 and assign value of 2.53e-9, or divide the velocity between the ends for the velocity boundary conditions
- For slip on the fault, resolve the slip into component vectors in the 1- and 2-directions and apply as a displacement boundary condition

Job

- Create Job, assign name

- Check full analysis
- Run job

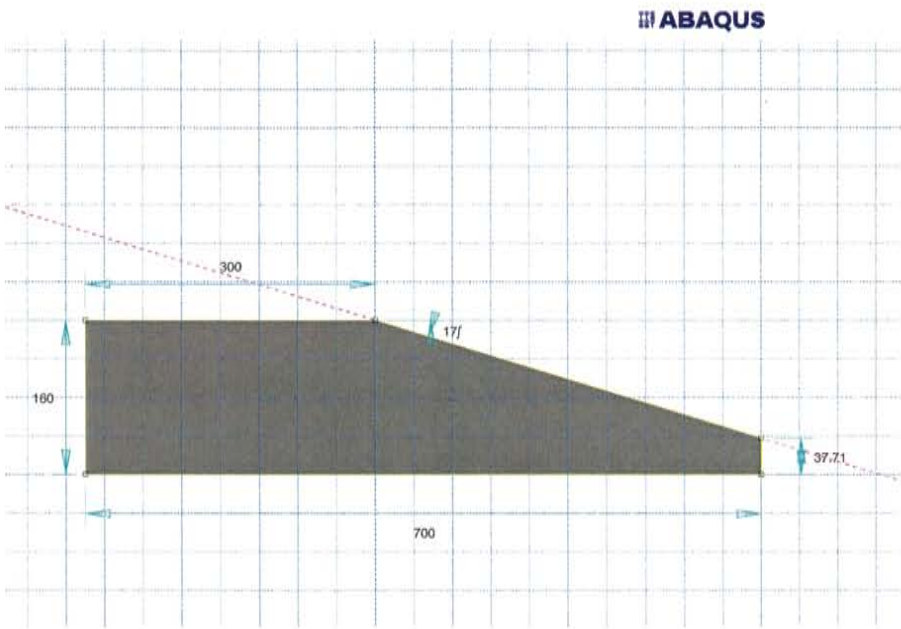

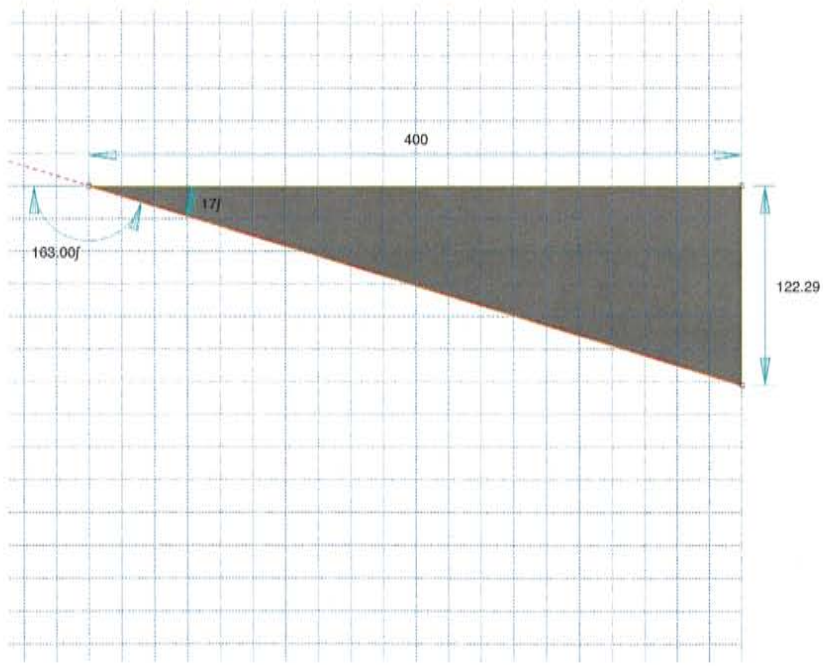

To change the model to a viscous creep model, we simply added the viscous creep component in the material properties editor, under the plastic option. The value for dynamic viscosity used was 56 GPa [*Masterlark*, 2003]We used strain-hardening with values of n=1 and m=0, for the orders for strain and time [Kenner, doctoral thesis, 2000]. Time-hardening is also available by changing the order of the derivatives in the differential equations. ABAQUS discussed the equations used and the theory behind them in the online Theory manual.

Meshing is perhaps the most difficult feature to resolve. Several meshing options are available in ABAQUS CAE, but for certain geometries it lacks flexibility. Many users opt to create their own meshing script, particularly with more complex 3-D geometries. In this 2-D application, I used a tetrahedral CAE meshing option, and the mesh was relatively fine, but with a 2-D simple model it did not affect computation time significantly. My first attempts were to use a quadrilateral mesh, but the mesh angles were either too great or too small, and instabilities ensued. The tetrahedral mesh model ran with no warnings or errors.

The primary problem with the model described above, was that the block was not restricted on the right hand side of the model. Thus, the model could translate in the positive 1 (x-) direction. I resolved this issue by dividing the velocity boundary conditions between the upper and lower blocks of the model. This allowed the blocks a more realistic "convergence" and solved the translation problem. I also revised the model to simulate more realistic rheologies by dividing each block into an upper and lower portion. The upper 40 kilometers of each block is assigned linear elastic properties, and the lower portion is assigned a viscous creep component. I decided to use 40 kilometers

depth for the upper portion in order to correspond to the seismogenic zone of the subduction interface [*DeShon et al.*, 2006]. The division of the blocks is accomplished by using the partition tool sketch option. Once the blocks are partitioned, it is possible to assign the individual rheologies to each section by creating the sections and using section assignments. I recommend using descriptive nomenclature rather than default, since using multiple materials and sections can become confusing if you don't remember which is which.

APPENDIX B

The following is a Matlab code which was used to compute Coulomb static stress changes from ABAQUS 2-D model results. Each timed run was computed for both viscous and elastic models. All Coulomb stress change calculations were computed as follows.

```
clear;
load elastic_e.rpt
%loading columns of results from ABAQUS
%each variable is a stress change value (e.g. %sig_a=S11, sig_b=S22,tau=S12)
sig_a=(elastic_e(:,3));
sig_b=(elastic_e(:,4));
tau=(elastic_e(:,5));
num=(elastic_e(:,1));
%calculate normal stress with angle of 11 degrees
norm=(sig_a+sig_b)./2-(sig_a-sig_b).*cos(2*11)./2+tau.*sin(2*11);
%calculate shear stress
shear=(sig_a-sig_b).*sin(2*11)./2+tau.*cos(2*11);
f=0.4;
%f is the friction coeff
%now calculate coulomb stress change
coul=(shear+f.*norm).*10^-8;
plot(num,coul,'r*')
hold on

load viscous_e.rpt
alpha=(viscous_e(:,3));
beta=(viscous_e(:,4));
zeta=(viscous_e(:,5));
count=(viscous_e(:,1));
v_norm=(alpha+beta)./2-(alpha-beta).*cos(2*11)./2+zeta.*sin(2*11);
v_shear=(alpha-beta).*sin(2*11)./2+zeta.*cos(2*11);
v_coul=(v_shear+f.*v_norm)*10^-8;
plot(count,v_coul,'c+')
hold off
```

APPENDIX C

Coulomb input file

nicoya-1990rerevised
trying new stress parameters
#reg1= 0 #reg2= 0 #fixed= 1 sym= 1
PR1= 0.25 PR2= 0.25 DEPTH= 20.
E1= 8.e+5 E2= 8.e+5
XSYM= .000 YSYM= .000
FRIC= 0.4
S1DR= 27. S1DP= 7. S1IN= 50. S1GD= 0.
S2DR= 113.98 S2DP= -3. S2IN= 45. S2GD= 0.
S3DR= 30.02 S3DP= 82. S3IN= .000000 S3GD= 0.

x-start y-start x-finish y-finish kode right-lat. reverse dip top bottom reference
xxx xxxxxxxxxx xxxxxxxxxx xxxxxxxxxx xxxxxxxxxx xxx xxxxxxxxxx xxxxxxxxxx xxxxxxxxxx xxxxxxxxxx xxxxxxxxxx
1 87. 41. 42. 62. 100 0. 2.34 11. 15. 30. fault-1
2 125.43 99.16 133.68 86.35 100 0. 0. 90. 0. 25. receiver fault-1

Grid Parameters
1 ---------- Start-x = 0.
2 ---------- Start-y = -45.
3 ---------- Finish-x = 255.
4 ---------- Finish-y = 175.
5 ---------- x-increment = 2.
6 ---------- y-increment = 2.
Size Parameters
1 ---------- Plot size = 1.
2 ---------- Shade/Color increment = 0.2
3 ------ Exaggeration for disp.& dist. = 1000.

REFERENCES CITED

Aki, K. (1979), Characterization of barriers on an earthquake fault, *Journal of Geophysical Research*, *84*, 6140-6148.

Aki, K. (1984), Asperities, barriers, characteristic earthquakes and strong motion prediction (Japan), *Journal of Geophysical Research*, *89*, 5867-5872.

Barckhausen, U., H. A. Roeser, and R. von Huene (1998), Magnetic signature of upper plate structures and subducting seamounts at the convergent margin off Costa Rica, *Journal of Geophysical Research*, *103*, 7079-7093.

Bilek, S. L., S. Y. Schwartz, and H. R. DeShon (2003), Control of seafloor roughness on earthquake rupture behavior, *Geology*, *31*, 455-458.

Byerlee, J. (1978), Friction of Rocks, *Pure and Applied Geophysics*, *116*, 615-626.

Byrne, T., and J. Hibbard (1987), Landward vergence in accretionary prisms: The role of the backstop and thermal history, *Geology*, *15*, 1163-1167.

Cloos, M. (1992), Thrust-type subduction-zone qarthquakes and seamount apserities: A physical model for seismic rupture, *Geology*, *20*, 601-604.

DeMets, C. (2001), A new estimate for present-day Cocos Caribbean plate modtion: Implications for slip along the Central American volcanic arc, *Geophysical Research Letters*, *28*, 4043-4046.

DeShon, H. R., S. Y. Schwartz, A. V. Newman, V. Gonzales, M. Protti, L. M. Dorman, T. H. Dixon, D. E. Sampson, and E. R. Flueh (2006), Seismogenic zone structure beneath

the Nicoya Peninsula, Costa Rica, from three-dimensional local earthquake P- and S-wave tomography, *Geophysical Journal International*, *164*, 109-124.

Dominguez, S., S. E. Lallemand, J. Malavieille, and R. von Huene (1998), Upper plate deformation associated with seamount subduction, *Tectonophysics*, *293*, 207-224.

Fisher, D., T. W. Gardner, J. S. Marshall, P. B. Sak, and M. Protti (1998), Effect of subducting sea-floor roughness on fore-arc kinematics, Pacific coast, Costa Rica, *Geology*, *26*, 476-470.

Freed, A. M. (2005), Earthquake Triggering by Static, Dynamic, and Postseismic Stress Transfer, *Annual Reviews in Earth and Planetary Science*, *33*, 335-367.

Hinz, K., R. von Huene, C. R. Ranero, and P. W. Group (1996), Tectonic structure of the convergent Pacific margin offshore Costa Rica from multichannel seismic reflection data, *Tectonics*, *15*, 54-66.

Honda, S., M. Saito, and T. Nakakuki (2002), Possible existence of small-scale convection under the back arc, *Geophysical Research Letters*, *29*, 391-394.

Husen, S., E. Kissling, and R. Quintero (2002), Tomographic evidence for a subducted seamount beneath the Gulf of Nicoya, Xosta Rica: The cause of the 1990 Mw=7.0 Gulf of Nicoya earthquake, *Geophysical Research Letters*, *29*.

Johnson, L. R., and R. M. Nadeau (2002), Asperity model of an earthquake: Static problem, *Bulletin of the Seismological Society of America*, *92*, 672-686.

Johnson, L. R., and R. M. Nadeau (2005), Asperity model of an earthquake: Dynamic problem, *Bulletin of the Seismological Society of America*, *95*, 75-108.

Kanamori, H. (1986a), Rupture Process of Subduction-Zone Earthquakes, *Annual Reviews in Earth and Planetary Science*, *14*, 293-322.

Kanamori, H. (1986b), *Rupture process of subduction-zone earthquakes*, 293-322 pp.

Kenner, S. (2000), Mechanical Modeling of Time Dependent Deformation in the Lower Crust and its Effect on Earthquake Recurrence.

Kenner, S., and P. Segall (1999), Time-dependence of the stress shadowing effect and its relation to the structure of the lower crust, *Geology*, *27*, 119-122.

King, G. C. P., R. Stein, and J. Lin (1994), Static stress changes and the triggering of earthquakes, *Bulletin of the Seismological Soceity of America*, *84*, 935-953.

Lay, T., H. Kanamori, and L. Ruff (1982), The asperity model and the nature of large subduction zone earthquakes, *Earthquake Prediction Research*, *1*, 3-71.

Lay, T., H. Kanamori, and L. J. Ruff (1981), The Asperity Model and the Nature of Large Subduction Zone Earthquakes, *1*, 3-71.

Lin, J., and R. Stein (2004), Stress triggering in thrust and subduction earthquakes and stress interaction betreen the southern San Andreas and neraby thrust and strike-slip faults, *Journal of Geophysical Research*, *109*.

Lundgren, P., M. Protti, A. Donnellan, M. Heflin, E. Hernandez, and D. Jefferson (1999), Seismic cycle and plate margin deformation in Costa Rica: GPS observations from 1994 to 1997, *Journal of Geophysical Research*, *104*, 28,925-928,926.

Marshall, J. S., D. Fisher, and T. W. Gardner (2000a), Central Costa Rica deformed belt: Kinematics of diffuse faulting across the western Panama block, *Tectonics*, *19*, 468-492.

Marshall, J. S., D. M. Fisher, and T. W. Gardner (2000b), Central Costa Rica deformed belt: Kinematics of diffuse faulting across the western Panama block, *Tectonics*, *19*, 468-492.

Masterlark, T. (2003), Finite element model predictions of static deformation from dislacation sources in a subdcution zone: Sensitivities to homogeneous, isotropic, Poisson-solid, and half-space assumptions, *Journal of Geophysical Research*, *108*.

Masterlark, T., C. DeMets, H. F. Wang, O. Sanchez, and J. Stock (2001), Homogeneous vs heterogeneous subduction zone models: Coseismic and postseismic deformation, *Geophysical Research Letters*, *28*, 4047-4050.

Norabuena, E., T. H. Dixon, S. Y. Schwartz, H. R. DeShon, A. V. Newman, M. Protti, V. Gonzales, L. M. Dorman, E. R. Flueh, P. Lundgren, F. Pollitz, and D. E. Sampson (2004), Geodetic and seismic constraints on some seismogenic zone processes in Costa Rica, *Journal of Geophysical Research*, *109*.

Parsons, T. (2005), A hypothesis for delayed dynamic earthquake triggering, *Geophysical Research Letters*, *32*.

Protti, M., V. Gonzales, U. Barckhausen, R. von Huene, C. DeMets, and S. Husen (1995a), The March 25, 1990 (M(w)=7.0, M(l)=6.8), earthquake at the entrance of the Nicoya Gulf, Costa-Rica - its prior activity, foreshocks, aftershocks, and triggered seismicity, *Journal of Geophysical Research*, *100*, 20345-20358.

Protti, M., F. Guendel, and K. McNally (1995b), Correlation between the age of the subducting Cocos palte and the geometry of the Wadati-Benioff zone under Nicaragua and Costa Rica, *Geological Society of America Special Paper*, *295*, 309-326.

Protti, M., K. McNally, J. Pacheco, V. Gonzalez, C. Montero, J. Segura, J. Brenes, V. Barboza, E. Malavassi, F. Guendel, G. Simila, D. Rojas, A. Velasco, A. Mata, and W. Schillinger (1995c), THE MARCH 25, 1990 (M(W)=7.0, M(L)=6.8), EARTHQUAKE AT THE ENTRANCE OF THE NICOYA GULF, COSTA-RICA - ITS PRIOR ACTIVITY, FORESHOCKS, AFTERSHOCKS, AND TRIGGERED SEISMICITY, *Journal of Geophysical Research-Solid Earth*, *100*, 20345-20358.

Ruff, L. J. (1992), Asperity distributions and large earthquake occurence in subduction zone, *Tectonophysics*, *211*, 61-83.

Ruff, L. J. (2001), Stress on the seismogenic and deep creep interface during the earthquake cycle in subduction zones, *Earth Planets Space*, *53*, 307-320.

Saito, S. and D. Goldberg (2001). Compaction and dewatering processes of the oceanic sediments in the Costa Rica and Barbados subduction zones; estimates from in situ physical property measurements. Earth and Planetary Science Letters, no. 3-4: 283-293.

Spinelli, G.A. and D.M. Saffer (2006). Hydrogeologic responses to three-dimensional temperature variability, Costa Rica subduction margin, *Journal of Geophysical Research*, B4.

Steacy, S., J. Gomberg, and M. Cocco (2005a), Introduction to special session:Stress transfer, earthquake triggering, and time-dependent seismic hazard, *Journal of Geophysical Research, 110.*

Steacy, S., D. Marsan, S. S. Nalbant, and J. McCloskey (2004), Sensitivity of static stress calculations to the earthquake slip distribution, *Journal of Geophysical Research, 109.*

Steacy, S., S. S. Nalbant, J. McCloskey, C. Nostro, O. Scotti, and D. Baumont (2005b), Onto what planes should Coulomb stress perturbations be resolved? *Journal of Geophysical Research-Solid Earth, 110*, B05S15.

Stein, R., G.C.P. King (1992), Changes in Failure Stress on the Southern San Andreas Fault System Caused by the Magnitude = 7.4 Landers Earthquake. *Science, 258* :1328-1332.

Stein, R. (1999), The role of stress transfer in earthquake occurrence, *Nature, 402*, 605-609.

Stein, R., A. A. Barka, and J. H. Dieterich (1997), Progressive failure on the North Anatolian fault since 1939 by earthquake stress triggering, *Geohpysical Journal International, 128*, 594-604.

Taylor, M. A. J., R. Dmowska, and J. R. Rice (1998a), *Upper plate stressing adn seismicity in the subduction earthquake cycle, 103*, 24,523-524,542.

Taylor, M. A. J., R. Dmowska, and J. R. Rice (1998b), Upper plate stressing and seismicity in the subduction earthquake cycle, *Journal of Geophysical Research-Solid Earth, 103*, 24523-24542.

Taylor, M. A. J., G. Zheng, J. R. Rice, W. D. Stuart, and R. Dmowska (1996), Cyclic stressing and seismicity at strongly coupled subduction zones, *Journal of Geophysical Research-Solid Earth, 101*, 8363-8381.

Toda, S., and R. Stein (2002), Response of the San Andreas fault to the 1983 Coalinga-Nunez earthquakes: An application of interaction-based probabilities for Parkfield, *Journal of Geophysical Research, 107*, 2126.

Vannucchi, P., D.W. Scholl (2001). Tectonic erosion and consequent collapse of the Pacific margin of Costa Rica; combined implications from ODP Leg 170, seismic offshore data, and regional geology of the Nicoya Peninsula. Tectonics, 20 (no.5): 649-668.

von Huene, R., J. Bialas, E. R. Flueh, B. Cropp, C. T., E. Fabel, J. Hoffmann, K. Emeis, P. Holler, G. Jeschke, C. Leandro, I. Perez Fernandez, and S. Chavarria (1995), Morphotectonics of the Pacific convergent margin of Costa Rica, *Geological Society of America Special Paper, 295*, 291-307.

Ziv, A., and A. M. Rubin (2000), Static stress transfer and earthquake triggering: No lower threshold in sight? *Journal of Geophysical Research-Solid Earth, 105*, 13631-13642.